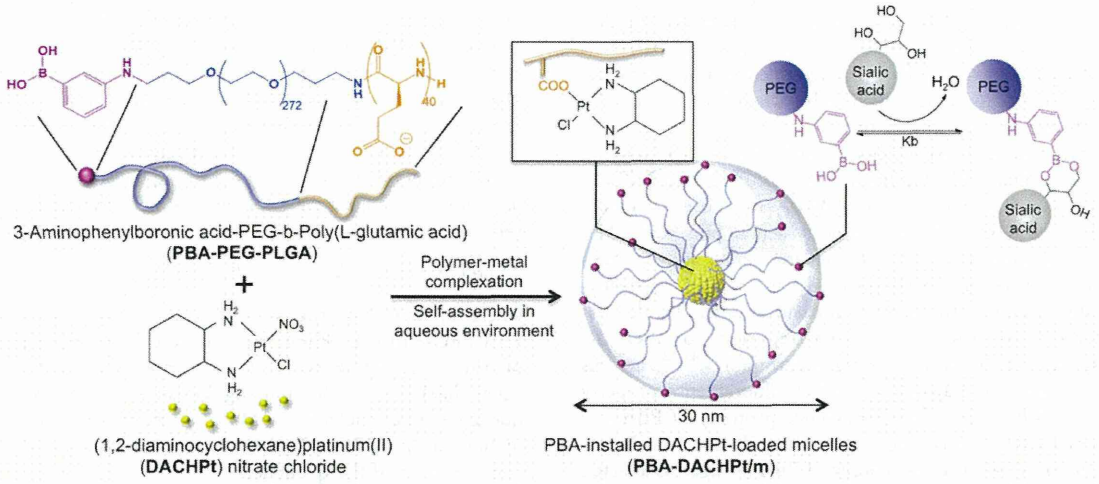

Figure 1. Preparation of PBA-installed DACHPt-loaded micelles by self-assembly through polymer–metal complex formation between DACHPt and PBA-poly(ethylene glycol)-*b*-poly(L-glutamic acid) in distilled water. PBA moieties on the surface of the micelles can bind to SA.

targeted *in vitro* by using lectin[19] and antibodies,[20] such as the tumoral marker CA19-9, used for detection of Sialyl-Lewis[a] in gastrointestinal tumors. Nevertheless, these approaches have been difficult to translate *in vivo*, mainly because of their immunogenicity. Moreover, as SA is also present on red blood cells and the luminal surfaces of vascular endothelium,[21,22] systemically injected ligands for SA targeting should not be active until reaching the site of tumors.

We have recently demonstrated the ability of phenylboronic acid (PBA) for selective recognition of SA overexpressed on the surface of cancer cells.[23] Although PBA can also form complexes with other common sugars, they are unstable unless formed at pHs higher than its pK_a value, whereas the complex between PBA and SA is stable even at pHs lower than its pK_a.[24,25] This feature, with controlled pK_a of PBA, provides a molecular basis for the specific SA recognition at physiological pH. This interaction has been recently used for determining the sialylation status of solid tumors by MRI through PBA-based reporters.[26] In addition to the high affinity and selectivity for SA, PBA presents several advantages for targeting of cancer cells such as being nontoxic, nonimmunogenic, and inexpensive.

Herein, we developed PBA-functionalized nanocarriers by installing PBA moieties on the polymeric micelles for specific targeting of SA epitopes overexpressed on tumor cells. Polymeric micelles, i.e., core–shell self-assemblies of block copolymers, provide multiple advantages as nanocarriers including their nanoscaled size, their poly(ethylene glycol) (PEG) shell, which prevents their recognition by macrophages of the reticuloendothelial system (RES) and prolongs their blood circulation time, and hydrophobic core for loading and controlled release of bioactive molecules.[4,5,27−29] Our polymeric micelles incorporating the anticancer drugs paclitaxel, SN-38, cisplatin, and the parent complex of oxaliplatin, i.e., dichloro(1,2-diamino-cyclohexane)platinum(II) (DACHPt), have advanced to clinical studies,[30,31] demonstrating high efficacy against several intractable tumors, such as triple-negative breast cancers, and less side effects in patients.[30] In this study, we use DACHPt-loaded micelles (DACHPt/m), which have shown selective accumulation in tumor tissues and strong suppression of the growth of several tumor models,[32−35] to prepare polymeric micelles having PBA moieties on their surface. The micelles were self-assembled through the coordination bond between platinum drug and the carboxylic groups of PBA-poly(ethylene glycol)-*b*-poly(L-glutamic acid) [PBA-PEG-*b*-PLGA] copolymers in water (Figure 1). The inherent fluorescence of PBA installed to PEG-*b*-PLGA copolymers was used for studying its binding affinity against different sugars by fluorescence spectroscopy. Moreover, the ability of PBA-installed DACHPt/m (PBA-DACHPt/m) to target SA in tumors was evaluated *in vitro* as well as *in vivo* against orthotopic and metastatic tumor models. For this purpose, highly metastatic B16F10 murine melanoma cells overexpressing SA on their surface[36] were used, for which we have recently established a method of quantification based on the PBA-SA interaction.[23] Our results showed a high selectivity of PBA-DACHPt/m to SA epitopes, which enhanced their cellular uptake *in vitro* and improved their tumor accumulation and retention *in vivo*, leading to a superior antitumor effect.

■ RESULTS AND DISCUSSION

Preparation of PBA End-Functionalized PEG-*b*-PLGA. Acetal-poly(ethylene glycol)-*b*-poly(L-glutamic acid) [acetal-PEG-*b*-PLGA] block copolymer was reacted with 3-aminophenylboronic acid by one pot reductive amination to afford aminophenylboronic acid-poly(ethylene glycol)-*b*-poly(L-glutamic acid) [PBA-PEG-*b*-PLGA] copolymer (Scheme S1). Thus, after deprotection of the acetal residue under acidic conditions, the obtained aldehyde group formed a Schiff base with 3-amino-substituted PBA. This intermediate imine was reduced to a secondary amine by using $NaBH_3CN$. The PBA installation at PEG end was confirmed to be almost quantitative by the proton ratios of the aromatic group of PBA and the ethylene units in PEG in the ^1H NMR spectrum (Figure S1).

Binding Affinities of PBA-PEG-*b*-PLGA to Various Sugars. Most sugars can complex only with the tetrahedral anionic form of boronate, because the complex with the trigonal neutral form is usually susceptible to hydrolysis.[37] In contrast, SA-PBA complexation is also favored by the trigonal form, for which involvement of multiple metastable binding sites along with intramolecular stabilization via B–N or B–O interactions are likely to play roles.[24,38,39] The pK_a value of the

polymer conjugated PBA, as assessed by fluorescence titration (Figure S2), was determined to be 9.7. This value, which is safely higher than that of physiological conditions, indicates predominant fraction of trigonal (undissociated) PBA at pH 7.4 and, thus, warrants specificity to SA.

To demonstrate the specificity of the PBA modified polymer for SA, we evaluated the binding affinities of PBA-PEG-*b*-PLGA for a series of sugars, such as glucose, mannose, galactose, Neu5Ac, and 2-O-methyl-α-D-*N*-acetylneuraminic acid (Me-Neu5Ac; Me-SA), which is a model for neuraminic residues present in the terminal positions of glycan chains,[40] by steady-state fluorescence quenching measurements. While the complexation of sugars has been reported to alter the fluorescence of boron-containing fluorophores,[41,42] in this study, we took advantage of the intrinsic fluorescence property of PBA-PEG-*b*-PLGA. The fluorescence property of PBA was maintained after PBA conjugation to the polymer end (Figure 2A). Moreover, because the binding of PBA to sugars is affected by pH,[37] we perform the experiments at pH 7.4, i.e., physiological pH, and at pH 6.5, which is the lowest environmental pH found inside tumors.[43] The fluorescence spectra of PBA-PEG-*b*-PLGA were collected in the presence of glucose, galactose, mannose, or Neu5Ac. Figure 2B shows the representative fluorescence spectra of PBA-PEG-*b*-PLGA on addition of Neu5Ac at pH 7.4, illustrating a quenching of fluorescence to occur due to photoinduced electron transfer (PET) as a result of the PBA-Neu5Ac complexation.[44,45] Accordingly, the relative fluorescence intensities of PBA-PEG-*b*-PLGA as a function of sugar concentration at pH 7.4 are shown in Figure 2C and at pH 6.5 in Figure 2D. The kinetic of the fluorescence quenching follows the Stern–Volmer equation (eq 1):

$$I_0/I = 1 + K_b\cdot[Q] = 1 + k_q''\cdot\tau_0\cdot[Q] \quad (1)$$

where I_0 represents the initial fluorescence intensity of the PBA-PEG-*b*-PLGA without sugar, I is the fluorescence intensity of the PBA-PEG-*b*-PLGA in the presence of the sugar (quencher), K_b is the binding constant (M^{-1}), k_q is the quencher rate coefficient ($M^{-1}s^{-1}$), τ_0 is the fluorescence lifetime of PBA-PEG-*b*-PLGA without quencher, and [Q] is the concentration of the quencher.

The binding constants are given as a slope in the Stern–Volmer plot (Figure 2C,D) and reported in Table 1.

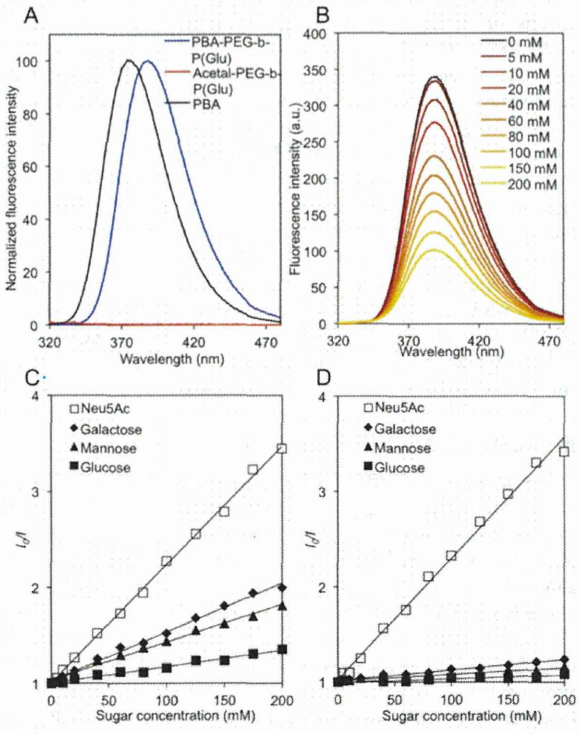

Figure 2. (A) Emission spectra of PBA, Acetal-PEG-*b*-PLGA and PBA-PEG-*b*-PLGA in phosphate buffer (0.1 M, pH 7.4) at room temperature, λ_{ex} = 302 nm. B. Emission spectra of PBA-PEG-*b*-PLGA (40 μM) in phosphate buffer solution (0.1 M, pH 7.4) containing various concentrations of Neu5Ac (0–200 mM) at room temperature, λ_{ex} = 302 nm. Relative fluorescence as a function of sugar concentration for PBA-PEG-*b*-PLGA measured in phosphate buffer (0.1 M) at room temperature (λ_{ex} = 302 nm and λ_{em} = 388 nm) at pH 7.4 (C) and pH 6.5 (D). I_0 and I represent the fluorescence intensity in the absence and presence of sugar respectively. Data were fit according to Stern–Volmer equation (eq 1).

Table 1. Binding Constants and Rate Coefficients of PBA-PEG-*b*-PLGA and Sugars in Phosphate Buffer pH 7.4 and 6.5[a]

sugar		pH 7.4	pH 6.5	K_b 6.5/ K_b 7.4
glucose	K_b (M^{-1})	1.71	0.39	0.29
	$k_q \times 10^{-9}$ ($M^{-1}\cdot s^{-1}$)	0.18	0.04	–
mannose	K_b (M^{-1})	3.95	0.70	0.17
	$k_q \times 10^{-9}$ ($M^{-1}\cdot s^{-1}$)	0.41	0.07	–
galactose	K_b (M^{-1})	5.11	1.11	0.21
	$k_q \times 10^{-9}$ ($M^{-1}\cdot s^{-1}$)	0.53	0.11	–
Neu5Ac (SA)	K_b (M^{-1})	12.3	12.7	1.03
	$k_q \times 10^{-9}$ ($M^{-1}\cdot s^{-1}$)	1.28	1.32	–
MeNeu5Ac (Me-SA)	K_b (M^{-1})	3.40	6.00	1.76
	$k_q \times 10^{-9}$ ($M^{-1}\cdot s^{-1}$)	0.35	0.62	–

[a]Determined by steady-state fluorescence quenching measurements; τ_0 (ns) at pH 7.4 was 9.62 ± 49.2 and at pH 6.5 was 9.67 ± 49.2.

Furthermore, the quencher rate coefficients were assessed from the fluorescence lifetimes (Table 1), which remained unchanged for these pHs (6.5 and 7.4). We observed that the binding constants and the quencher rate coefficients were remarkably higher for Neu5Ac than those for other sugars, indicating a stronger affinity for SA. The binding constant values showed similar tendency with previously reported values using other boronic acids and different methods (UV,[46] ^{11}B-NMR,[24] or indirect fluorescence through the fluorescent reporter compound, Alizarin Red S[47]). Moreover, even though the affinity for sugars depends on the nature of boronic acid, a trend for the selectivity was noticed as SA ≫ galactose ≥ mannose ≅ glucose. It is worth noticing that the ratio between the binding constant at intratumoral pH, i.e., K_b 6.5, and that for pH 7.4, i.e., K_b 7.4, is maintained close to 1 for Neu5Ac, while it is <1 for others (Table 1), suggesting a higher binding efficiency of PBA for SA in the intratumoral environment. Moreover, the presence of a methyl group at the C2 hydroxyl

group of Me-SA reduced the binding constant, K_b, from 12.3 M^{-1} for SA to 3.4 M^{-1} for MeSA at pH 7.4 (Table 1). At pH 6.5, even though K_b decreased from 12.7 M^{-1} for SA to 6 M^{-1} for Me-SA, this binding constant was higher than the binding constants for the other sugars, indicating the selectivity of PBA for biological relevant SA at intratumoral pH (Table 1). Moreover, as K_b for Me-SA is higher at intratumoral pH than at physiological pH, it is expected that while the complex between PBA and SA will compete with other sugars in the bloodstream (pH 7.4), the PBA-installed micelles would primarily target SA under increasingly acidic conditions relevant to the environment of tumors.

Preparation and Characterization of PBA-Installed DACHPt-Loaded Micelles. Micelles were self-assembled due to the metal–polymer complexation between the carboxylic group of the PLGA and the platinum of DACHPt (Figure 1). Dynamic light scattering (DLS) measurements showed that the diameters of DACHPt/m and PBA-DACHPt/m were comparable, i.e., ~30 nm by weight distribution (Figure 3 and Table 2). Accordingly, these diameters may be suitable for achieving deep penetration in solid tumors, as we have recently demonstrated that 30 nm DACHPt/m can deeply penetrate even in poorly permeable malignancies.[35] Both micelles also showed comparable ζ potential values, which were slightly negative at pH 7.4 (Table 2). The Pt content in both micelles was found to be similar and remarkably high (Table 2), as determined by inductively coupled plasma mass spectrometry (ICP-MS). Moreover, in media containing chloride ions, i.e., 10 mM PBS plus 150 mM NaCl, DACHPt is released from the core of the micelles by exchange reaction between chloride ions and carboxylic groups of PLGA.[32−34] Accordingly, the conjugation of PBA ligands did not affect the drug release rate of the micelles, and both DACHPt/m and PBA-DACHPt/m released ~40% of DACHPt after 2 days (Figure S3), which is similar to our previous reports.[32−34]

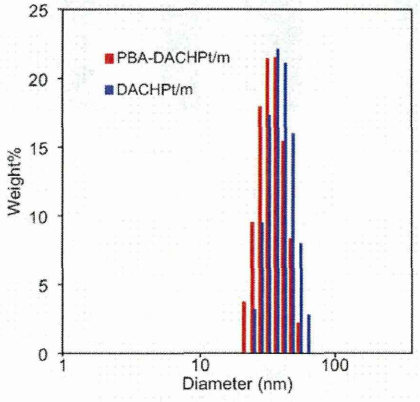

Figure 3. Diameter of DACHPt/m and PBA-DACHPt/m by weight distribution determined by DLS.

Table 2. Diameter, Polydispersity, Drug Loading and ζ Potential of DACHPt/m and PBA-DACHPt/m

	DACHPt/m	PBA-DACHPt/m
diameter[a] (nm)	35	29
polydispersity index[a]	0.1	0.1
ζ potential (mV)[b]	−2.3 ± 1.4	−5.7 ± 0.3
Pt/polymer (wt/wt %)[c]	30	31
[Pt]/[COO] (mol/mol %)[c]	50	52

[a]Determined by weight% distribution obtained with DLS. [b]Determined in 10 mM phosphate buffer, pH 7.4. [c]Determined by ICP-MS.

***In vitro* Targeting Ability of PBA-Installed DACHPt-Loaded Micelles.** The ability of PBA-DACHPt/m to bind SA epitopes in cancer cells was studied *in vitro*. First, we evaluated the cellular uptake of fluorescent-labeled micelles in B16F10 murine melanoma cells, which overexpress SA on the membrane,[23,36] by confocal laser microscopy. For constructing the fluorescent-labeled micelles, we conjugated Alexa Fluor 555 succinimidyl ester to the ω-amino group of MeO-PEG-*b*-PLGA and PBA-PEG-*b*-PLGA and obtained MeO-PEG-*b*-PLGA-$Alexa_{555}$ and PBA-PEG-*b*-PLGA-$Alexa_{555}$. The conjugation degree of Alexa Fluor 555 was 4 mol % for both polymers. We built the fluorescent micelles following the same method as for unlabeled micelles. After micelle formation, the fluorescence signal from the Alexa Fluor 555 probes in the core of the micelles was still detectable. Thus, after incubating the cells with the fluorescent micelles for 3 h, the fluorescent signal of PBA-DACHPt/m was significantly higher than that of DACHPt/m, indicating a faster cellular uptake (Figure 4A,B). After 6 h incubation, the difference between the micelles became more evident, as the fluorescent signal from PBA-DACHPt/m was localized inside the cells, while the signal from DACHPt/m was barely detectable (Figure 4A,B). After 9 h incubation, even though the fluorescent DACHPt/m was detected inside the tumor cells due to nonspecific uptake (Figure 4A,B), the fluorescent signal of PBA-DACHPt/m was still significantly higher (Figure 4B; $p < 0.001$). The addition of free PBA to the cell culture media reduced the cellular uptake of PBA-DACHPt/m, which showed a similar intensity to DACHPt/m (Figure 4A,B), indicating that the enhanced cellular uptake of PBA-DACHPt/m is due to the interaction of PBA moieties with the cells. Furthermore, treating the cells with sialidase, which is an enzyme that can cleave SA epitopes from the cells, before incubation with the micelles, led to a drastic decrease of the cellular internalization of PBA-DACHPt/m (Figure 4A,B), demonstrating the specific interaction of these micelles with SA epitopes on the cell membrane. For both free PBA- and sialidase-treated cells, the intracellular signal of fluorescent-labeled PBA-DACHPt micelles increased after 9 h incubation, comparable to nontargeted DACHPt/m with fluorescent-labeling, probably due to nonspecific uptake.

The enhancement of the antitumor effect of PBA-installed micelles was determined by evaluating the 50% growth inhibitory concentration (IC_{50}) against B16F10 cells. Moreover, the activity of the micelles was compared with that of oxaliplatin, because it is the clinically approved DACHPt-derivative and presents the same active complexes as the micelles. After exposing the cells to oxaliplatin or micelles for 3 h, the cells were washed and postincubated for 48 h. Thus, while free oxaliplatin showed lower IC_{50} than both micelles, probably due to its rapid cellular internalization as well as the slow sustained release of DACHPt complexes from the micelles, the cytotoxicity of PBA-DACHPt/m was higher than that of DACHPt/m (Table 3), which correlated with the increased cellular uptake of these micelles, suggesting their potential for enhancing the therapeutic effect *in vivo*.

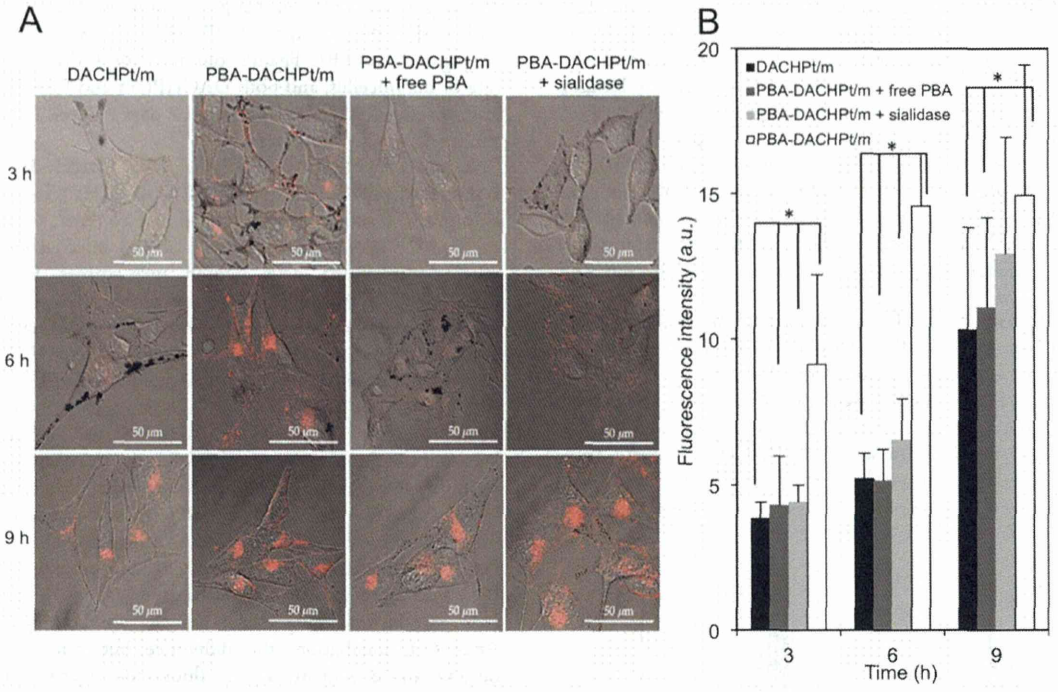

Figure 4. (A) Fluorescent microscopies of B16F10 cells incubated with fluorescent-labeled DACHPt/m or PBA- DACHPt/m for 3, 6, and 9 h. Free PBA was added 10 min before the addition of PBA- DACHPt/m for the competition assay. To cleave specifically SA, the cells were pretreated with sialidase before the incubation with PBA-DACHPt/m. The polymers were labeled with a fluorescent dye (Alexa Fluor 555; red). (B) Quantification of the fluorescence intensity. Data are expressed as averages ± S.E.M., $n = 20$, $^*p < 0.001$.

Table 3. *In vitro* Cytotoxicity of Free Oxaliplatin, DACHPt/m, and PBA-DACHPt/m after 48 h of Total Incubation Against B16F10 Cell Line

	IC_{50} (μM)[a]		
cells	oxaliplatin	DACHPt/m	PBA-DACHPt/m
B16F10	142 ± 5	278 ± 11	184 ± 8

[a]Determined by WST-8 assay ($n = 8$).

***In vivo* Targeting Ability of PBA-Installed DACHPt-Loaded Micelles.** The performance of the micelles was evaluated *in vivo* in mice bearing B16F10 melanoma tumors. Accordingly, intravenously injected DACHPt/m and PBA-DACHPt/m showed similar prolonged blood circulation with ~20% of injected dose per ml of plasma after 24 h (Figure 5A), which is in agreement with our previous results for DACHPt/m,[32,34,35] suggesting the reduced interaction of PBA-DACHPt/m with red blood cells and endothelial cells in the vasculature. This reduced interaction may be due to the interference by glucose in plasma, as normal glucose levels are ~5 mM, while the concentration of SA in erythrocytes (SA_{RBC}) is ~0.2 μM (20 nmol/10^9 cells).[48] Conversely, inside tumors, the glucose concentration decreases due to diffusion and the persistent metabolism of glucose to lactate in cancer cells.[49] Moreover, the metabolic products of this anaerobic glycolysis cause acidification of the intratumoral space, which decreases the binding constant for glucose (Table 1). Because the binding constant for SA at intratumoral pH is maintained and the SA amount on B16F10 cells is 1.1 nmol/10^6 cells,[23] which is more than 1000-fold higher than for erythrocytes, we expect that PBA-DACHPt/m effectively bind to tumor cells *in vivo*.

The tumor accumulation of DACHPt/m and PBA-DACHPt/m was similar up to 24 h, reaching ~5% of the injected dose per g of tissue. However, 48 h after injection, the amount of DACHPt/m in the tumors declined, whereas PBA-DACHPt/m maintained their accumulation level in the tumor (Figure 5B; $p < 0.05$), suggesting that the interaction of PBA-DACHPt/m with the SA moieties on the surface of cancer cells improved the retention of micelles at the tumor site. As this prolonged tumor retention increases the exposure of the cancer cells to anticancer drugs, it may enhance the antitumor activity of PBA-DACHPt/m.

The antitumor activity of PBA-DACHPt/m was evaluated in an orthotopic tumor model prepared by intradermal inoculation of B16F10 cells to mice ($n = 5$). Mice were treated with intravenous injection three times at 2 day intervals, i.e., at days 0, 2, and 4, with oxaliplatin at dose of 8 mg/kg, and DACHPt/m or PBA-DACHPt/m at a dose of 3 mg/kg. These doses were selected based on our previous observations for the maximum tolerated dose for oxaliplatin and the effective dose for DACHPt/m.[33] Thus, while free oxaliplatin failed to show any antitumor effect, probably due to its low accumulation in tumor tissues as well as its inactivation due to binding to serum proteins and erythrocytes after systemic administration,[50] both DACHPt/m and PBA-DACHPt/m significantly reduced the growth rate of the tumors, correlating with their enhanced accumulation in tumors (Figure 5B),with PBA-DACHPt/m showing higher efficacy than DACHPt/m ($p = 0.005$) (Figure 5C). Moreover, polymeric micelles can protect the Pt drug in their core during circulation and enhance the drug delivery to the nucleus of cancer cells,[34] therefore, increasing the *in vivo* antitumor efficacy of the Pt drug. In addition, this activity

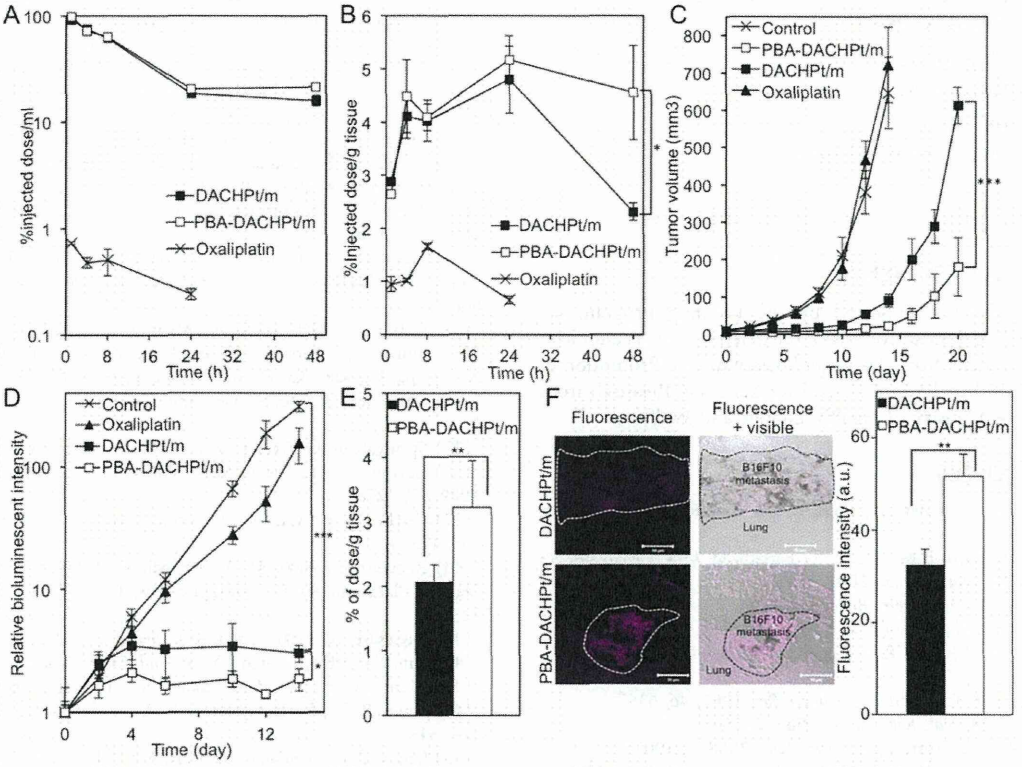

Figure 5. *In vivo* properties of PBA-DACHPt/m. (A) Plasma clearance and (B) tumor accumulation of DACHPt/m and PBA-DACHPt/m in mice bearing B16F10 tumor model. Data are means ± S.E.M.; $n = 5$; $^{*}p < 0.05$. (C) Antitumor activity against orthotopic B16F10 tumors after treatment with oxaliplatin (8 mg/kg), DACHPt/m or PBA-DACHPt/m (3 mg/kg) injected on days 0, 2, and 4. Data are expressed as averages ± S.E.M.; $n = 5$; $^{***}p < 0.001$. (D) Antitumor activity against lung metastasis induced by B16F10-Luc melanoma cells. Data are expressed as averages ± S.E.M.; $n = 5$; $^{*}p < 0.05$; $^{***}p < 0.001$. (E) Accumulation of micelles in lungs having B16F10-Luc melanoma cells 24 h after the intravenous injection. Data are expressed as averages ± S.E.M., $n = 6$, $^{**}p < 0.005$. (F) Ex vivo fluorescent microscopies of lung tissues bearing B16F10-Luc metastasis 24 h after the injection of fluorescent-labeled DACHPt/m or PBA-DACHPt/m (Alexa Fluor 647; pink) and quantification of fluorescent intensity in metastatic regions. Data are expressed as averages ± S.E.M., $n = 3$, $^{**}p < 0.005$.

enhancement did not come at the expense of side effects, and the body weight of the mice remained stable even after the repeated administration of the micelles (Figure S4).

In addition, as metastasis is the major cause of cancer-related death and because the expression of SA is highly associated with the metastatic disease,[18] we evaluated the efficiency of PBA-DACHPt/m against bioluminescent lung metastasis, obtained after intravenous injection of B16F10 cells expressing luciferase (B16F10-Luc) in BALB/c nu/nu mice. Mice were treated intravenously three times at 2 day intervals, i.e., at days 0, 2, and 4, with oxaliplatin at dose of 8 mg/kg, DACHPt/m or PBA-DACHPt/m at a dose of 3 mg/kg. By following the growth of metastasis through imaging the bioluminescence signal, we observed that, while oxaliplatin showed no antitumor effect (Figure 5D), both DACHPt/m and PBA-DACHPt/m significantly inhibited the progression of the metastasis. Again, PBA-DACHPt/m demonstrated to be more efficacious than DACHPt/m, showing 2-fold lower bioluminescent intensity (Figure 5D; $p < 0.05$). The enhanced activity of PBA-DACHPt/m matched the increased Pt accumulation of these micelles in metastatic lungs 24 h after injection (Figure 5E). Moreover, the specificity of PBA-DACHPt/m to the metastatic sites in lungs was confirmed by histology after the injection of micelles labeled with Alexa Fluor 647 (Figure 5F). Thus, the fluorescence intensity for PBA-DACHPt/m was higher than that for DACHPt/m at the metastatic regions, supporting the superior efficacy of PBA-DACHPt/m.

■ CONCLUSION

Our findings demonstrated that PBA conjugation of the surface of polymeric micellar nanocarriers enhanced their tumor targeting ability, by specific interaction with SA epitopes overexpressed in tumor cells, without affecting their long circulating properties. These results support the application of borate ester chemistry for specific targeting of tumor-associated carbohydrate antigens at intratumoral pH conditions. Moreover, because of the clear relationship between overexpression of sialylated epitopes, tumor aggressiveness, and patients' prognosis as well as the safety and nonimmunogenicity of the approach, PBA-mediated targeting of nanocarriers offers a highly translational approach for clinical diagnosis and therapy of solid tumors.

■ ASSOCIATED CONTENT

Supporting Information

Experimental section, preparation scheme, and ^{1}H NMR of PBA-PEG-*b*-PLGA, study of the pK_a of PBA-PEG-*b*-PLGA, the release rate profiles of the micelles and their *in vivo* toxicity are provided. This material is available free of charge via the Internet at http://pubs.acs.org.

AUTHOR INFORMATION

Corresponding Author

kataoka@bmw.t.u-tokyo.ac.jp

Author Contributions

◆These authors contributed equally.

Notes

The authors declare no competing financial interest.

ACKNOWLEDGMENTS

This research was supported by the Funding Program for World-Leading Innovative R&D on Science and Technology (FIRST Program) from the Japan Society for the Promotion of Science (JSPS) and Grants-in-Aid for Scientific Research from the Japanese Ministry of Health, Labour and Welfare.

REFERENCES

(1) Davis, M. E.; Chen, Z.; Shin, D. M. *Nat. Rev. Drug Discovery* **2008**, *7*, 771.
(2) Peer, D.; Karp, J. M.; Hong, S.; Farokhzad, O. C.; Margalit, R.; Langer, R. *Nat. Nanotechnol.* **2007**, *2*, 751.
(3) Duncan, R. *Curr. Opin. Biotechnol.* **2011**, *22*, 492.
(4) Nishiyama, N.; Kataoka, K. *Pharmacol. Ther.* **2006**, *112*, 630.
(5) Miyata, K.; Christie, R. J.; Kataoka, K. *React. Funct. Polym.* **2011**, *7*, 227.
(6) Matsumura, Y.; Maeda, H. *Cancer Res.* **1986**, *46*, 6387.
(7) Allen, T. M. *Nat. Rev. Cancer* **2002**, *2*, 750.
(8) Torchilin, V. *Expert Opin. Drug Deliv.* **2008**, *5*, 1003.
(9) Cheng, W. W.; Allen, T. M. *Expert Opin Drug Delivery* **2010**, *7*, 461.
(10) Farokhzad, O. C.; Cheng, J.; Teply, B. A.; Sherifi, I.; Jon, S.; Kantoff, P. W.; Richie, J. P.; Langer, R. *Proc. Natl. Acad. Sci. U.S.A.* **2006**, *103*, 6315.
(11) Zhang, X.-X.; Eden, H. S.; Chen, X. *J. Controlled Release* **2012**, *159*, 2.
(12) Oba, M.; Vachutinsky, Y.; Miyata, K.; Kano, M. R.; Ikeda, S.; Nishiyama, N.; Itaka, K.; Miyazono, K.; Koyama, H.; Kataoka, K. *Mol. Pharmaceutics* **2010**, *7*, 501.
(13) Bae, Y.; Jang, W. D.; Nishiyama, N.; Fukushima, S.; Kataoka, K. *Mol. Biosyst.* **2005**, *1*, 242.
(14) Hakomori, S. *Cancer Res.* **1996**, *56*, 5309.
(15) Dube, D. H.; Bertozzi, C. R. *Nat. Rev. Drug Discovery* **2006**, *4*, 477.
(16) Xu, Y.; Sette, A.; Sidney, J.; Gendler, S. J.; Franco, A. *Immunol. Cell Biol.* **2005**, *83*, 440.
(17) Kannagi, R.; Sakuma, K.; Miyazaki, K.; Lim, K. T.; Yusa, A.; Yin, J.; Izawa, M. *Cancer Sci.* **2010**, *101*, 586.
(18) Kannagi, R.; Izawa, M.; Koike, T.; Miyazaki, K.; Kimura, N. *Cancer Sci.* **2004**, *95*, 377.
(19) Sharon, N. *J. Biol. Chem.* **2007**, *282*, 2753.
(20) Koprowski, H.; Herlyn, M.; Steplewski, Z.; Sears, H. F. *Science* **1981**, *212*, 53.
(21) Durocher, J. R.; Payne, R. C.; Conrad, M. E. *Blood* **1975**, *45*, 11.
(22) Born, G. V.; Palinski, W. *Br. J. Exp. Pathol.* **1985**, *66*, 543.
(23) Matsumoto, A.; Cabral, H.; Sato, N.; Kataoka, K.; Miyahara, Y. *Angew. Chem., Int. Ed.* **2010**, *49*, 5494.
(24) Otsuka, H.; Uchimura, E.; Koshino, H.; Okano, T.; Kataoka, K. *J. Am. Chem. Soc.* **2003**, *125*, 3493.
(25) Djanashvili, K.; Frullano, L.; Peters, J. A. *Chem.—Eur. J.* **2005**, *11*, 4010.
(26) Geninatti Crich, S.; Alberti, D.; Szabo, I.; Aime, S.; Djanashvili, K. *Angew. Chem., Int. Ed.* **2013**, *52*, 1161.
(27) Kataoka, K.; Harada, A.; Nagasaki, Y. *Adv. Drug Delivery Rev.* **2001**, *47*, 113.
(28) Osada, K.; Christie, R. J.; Kataoka, K. *J. R. Soc. Interface* **2009**, *6*, S325.
(29) Cabral, H.; Kataoka, K. *Sci. Technol. Adv. Mater.* **2010**, *11*, 014109.
(30) Matsumura, Y.; Kataoka, K. *Cancer Sci.* **2009**, *100*, 572.
(31) Plummer, R.; Wilson, R. H.; Calvert, H.; Boddy, A. V.; Griffin, M.; Sludden, J.; Tilby, M. J.; Eatock, M.; Pearson, D. G.; Ottley, C. J.; Matsumura, Y.; Kataoka, K.; Nishiya, T. *Br. J. Cancer* **2011**, *104*, 593.
(32) Cabral, H.; Nishiyama, N.; Okazaki, S.; Koyama, H.; Kataoka, K. *J. Controlled Release* **2005**, *101*, 223.
(33) Cabral, H.; Nishiyama, N.; Kataoka, K. *J. Controlled Release* **2007**, *121*, 146.
(34) Murakami, M.; Cabral, H.; Matsumoto, Y.; Wu, S.; Kano, M. R.; Yamori, T.; Nishiyama, N.; Kataoka, K. *Sci. Transl. Med.* **2011**, *3*, 64ra2.
(35) Cabral, H.; Matsumoto, Y.; Mizuno, K.; Chen, Q.; Murakami, M.; Kimura, M.; Terada, Y.; Kano, M. R.; Miyazono, K.; Uesaka, M.; Nishiyama, N.; Kataoka, K. *Nat. Nanotechnol.* **2011**, *6*, 815.
(36) Kinoshita, Y.; Sato, S.; Takeuchi, T. *Cell. Struct. Funct.* **1989**, *14*, 35.
(37) Springsteen, G.; Wang, B. *Tetrahedron* **2002**, *58*, 5291.
(38) Levonis, S. M.; Kiefel, M. J.; Houston, T. A. *Chem. Commun.* **2009**, *17*, 2278.
(39) Teichert, J. F.; Mazunin, D.; Bode, J. W. *J. Am. Chem. Soc.* **2013**, *135*, 11314.
(40) Regueiro-Figueroa, M.; Djanashvili, K.; Esteban-Gómez, D.; de Blas, A.; Platas-Iglesias, C.; Rodríguez-Blas, T. *Eur. J. Org. Chem.* **2010**, 3237.
(41) DiCesare, N.; Lakowicz, J. R. *J. Phys. Chem. A* **2001**, *105*, 6834.
(42) Sun, X.-Y.; Liu, B.; Jiang, Y.-B. *Anal. Chim. Acta* **2004**, *515*, 285.
(43) Martin, G. R.; Jain, R. K. *Cancer Res.* **1994**, *54*, 5670.
(44) James, T. D.; Sandanayake, K. R. A. S.; Shinkai, S. *Nature* **1995**, *374*, 345.
(45) James, T. D.; Sandanayake, K. R. A. S.; Shinkai, S. *Angew. Chem., Int. Ed.* **1996**, *35*, 1919.
(46) Mori, Y.; Suzuki, A.; Yoshino, K.; Kakihana, H. *Pigm. Cell Res.* **1989**, *2*, 273.
(47) Tomsho, J. W.; Benkovic, S. J. *J. Org. Chem.* **2012**, *77*, 2098.
(48) Miller, A.; Sullivan, J. F.; Katz, J. H. *Cancer Res.* **1963**, *23*, 485.
(49) Gatenby, R. A.; Gillies, R. J. *Nat. Rev. Cancer* **2004**, *4*, 891.
(50) Graham, M. A.; Lockwood, G. F.; Greenslade, D.; Brienza, S.; Bayssas, M.; Game, E. *Clin. Cancer Res.* **2000**, *6*, 1205.

Targeted therapy of spontaneous murine pancreatic tumors by polymeric micelles prolongs survival and prevents peritoneal metastasis

Horacio Cabral[a], Mami Murakami[a], Hironori Hojo[b], Yasuko Terada[c], Mitsunobu R. Kano[d], Ung-il Chung[a,b], Nobuhiro Nishiyama[e,1], and Kazunori Kataoka[a,b,f,1]

Departments of [a]Bioengineering and [f]Materials Engineering, Graduate School of Engineering, University of Tokyo, Bunkyo-ku, Tokyo 113-8656, Japan; [b]Center for Disease Biology and Integrative Medicine, Graduate School of Medicine, University of Tokyo, Bunkyo-ku, Tokyo 113-0033, Japan; [c]SPring 8, Japan Synchrotron Radiation Research Institute, Sayo-cho, Sayo-gun, Hyogo 679-5198, Japan; [d]Department of Pharmaceutical Biomedicine, Graduate School of Medicine, Dentistry, and Pharmaceutical Sciences, Okayama University, Kita-ku, Okayama 700-8530, Japan; and [e]Polymer Chemistry Division, Chemical Resources Laboratory, Tokyo Institute of Technology, Midori-ku, Yokohama 226-8503, Japan

Edited by Joseph M. DeSimone, University of North Carolina, Chapel Hill, NC, and approved June 4, 2013 (received for review January 31, 2013)

Nanoscaled drug-loaded carriers are of particular interest for efficient tumor therapy as numerous studies have shown improved targeting and efficacy. Nevertheless, most of these studies have been performed against allograft and xenograft tumor models, which have altered microenvironment features affecting the accumulation and penetration of nanocarriers. Conversely, the evaluation of nanocarriers on genetically engineered mice, which can gradually develop clinically relevant tumors, permits the validation of their design under normal processes of immunity, angiogenesis, and inflammation. Therefore, considering the poor prognosis of pancreatic cancer, we used the elastase 1-promoted luciferase and Simian virus 40 T and t antigens transgenic mice, which develop spontaneous bioluminescent pancreatic carcinoma, and showed that long circulating micellar nanocarriers, incorporating the parent complex of oxaliplatin, inhibited the tumor growth as a result of their efficient accumulation and penetration in the tumors. The reduction of the photon flux from the endogenous tumor by the micelles correlated with the decrease of serum carbohydrate-associated antigen 19-9 marker. Micelles also reduced the incidence of metastasis and ascites, extending the survival of the transgenic mice.

chemotherapy | drug delivery | (1,2-diaminocyclohexane)platinum(II)

The development of effective targeted drug-loaded nanocarriers for treating cancer is a priority in biomedical technology (1–4). Nanocarriers accumulate selectively in tumor sites owing to the "enhanced permeability and retention (EPR) effect" (5), which is characterized by leaky blood vessels and impaired lymphatic drainage, thereby achieving improved antitumor activity. After systemic administration, nanocarriers need to extravasate, penetrate into the interstitial tissue, and target the cancer cells to exert their in vivo antitumor activity. Nevertheless, most of the in vivo evaluation of nanocarriers has been performed in animal models prepared by implantation of exogenous tumor cells into non–tumor-bearing animals, which has significant differences compared with the microenvironment of tumors in patients (6, 7). Features of the microenvironment of tumors affecting the penetration and accumulation of nanocarriers such as stromal cells, vasculature, lymphatics, and immune cells, are altered in human xenograft and mouse allograft preclinical cancer models. Moreover, particular clonal fractions of polyclonal tumors may be increased in such cancer models due to selective stresses during the cell culture or tissue explantation (6, 7). These differences in tumor cells and microenvironment are relevant for the assessment of therapeutics, as several anticancer agents with demonstrable activity in allografted or xenografted cancer models have been shown to be ineffective in a clinical situation (8, 9). Genetically engineered tumor models arise in situ where immune function, angiogenesis, and inflammatory processes can all interact normally with a gradually developing tumor, closely relating to the clinical setting of the disease (6, 7). Although these transgenic tumor models may be more appropriate for the evaluation of promising nanocarriers, only a few nanocarrier systems have been assessed on transgenic models so far (10–19), mainly for imaging purposes (15–19).

Polymeric micelles consisting of a drug-loaded hydrophobic core and poly(ethylene glycol) (PEG) hydrophilic shell are promising nanocarriers in the tumor-targeted therapy (4, 20). Polymeric micelles present exceptional advantages as nanocarriers, including their size (10–100 nm), high capability of cellular targeting, controllable drug release, longevity in the bloodstream, and effective accumulation in solid tumors after i.v. injection (4, 20). Our micellar formulations incorporating the anticancer agents paclitaxel, 7-Ethyl-10-hydroxy-camptothecin (SN-38), cisplatin, and (1,2-diaminocyclohexane)platinum(II) (DACHPt) have advanced to clinical studies (21, 22), demonstrating high efficacy against several intractable tumors, such as triple-negative breast cancers, and fewer side effects in patients (21). In this study, we investigated the tumor targeting ability and therapeutic efficacy of DACHPt-loaded micelles (DACHPt/m), which are under phase I clinical evaluation, against a spontaneous pancreatic cancer model. DACHPt/m are prepared by polymer–metal complexation between DACHPt and the carboxylic groups of biocompatible and biodegradable poly(ethylene glycol)-*b*-poly (glutamic acid) [PEG-*b*-P(Glu)] copolymers (Fig. 1) (23–27), while the active drug is released from the micelles as a result of the ligand substitution with the chloride in the medium. Because DACHPt/m presents sustained drug release and concomitant micelle dissociation with an induction period of ~8 h in the extracellular environment, the micelles can circulate stably in the bloodstream in a micelle form with minimal drug release and gradually release the drug after accumulating in solid tumors (25). Thus, DACHPt/m have shown remarkably higher antitumor activity than the clinically approved DACH-containing platinum drug, that is, oxaliplatin, reducing the growth rate of several xenografted tumor models, such as human cervical cancer (24), human colon cancer (25), human pancreatic cancer (26), and human gastric cancer (27), due to their prolonged blood circulation and enhanced tumor accumulation.

Pancreatic cancer is among the most fatal cancers, with an incidence rate that approximates its mortality rate (28). The all-

Author contributions: H.C. designed research; H.C. and M.M. performed research; Y.T., U.-i.C., N.N., and K.K. contributed new reagents/analytic tools; H.C., M.M., H.H., M.R.K., N.N., and K.K. analyzed data; and H.C. wrote the paper.

The authors declare no conflict of interest.

This article is a PNAS Direct Submission.

Freely available online through the PNAS open access option.

[1]To whom correspondence may be addressed. E-mail: kataoka@bmw.t.u-tokyo.ac.jp or nishiyama@res.titech.ac.jp.

This article contains supporting information online at www.pnas.org/lookup/suppl/doi:10.1073/pnas.1301348110/-/DCSupplemental.

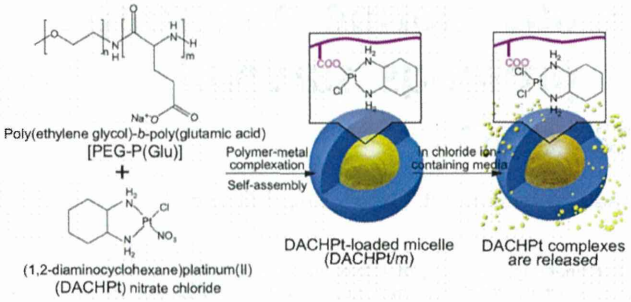

Fig. 1. Scheme of DACHPt/m preparation. DACHPt/m self-assembled through polymer–metal complex formation between DACHPt and poly (ethylene glycol)-*b*-poly(glutamic acid) in distilled water. In chloride ion-containing media, DACHPt is released from the micelles after an 8-h induction period (23, 25).

stage 5-y survival, which is 1–3%, has remained without change over the past 25 y (29); therefore, novel therapies that improve the prognosis of patients with advanced pancreatic cancer are urgently needed. In this study, we evaluated the efficacy of DACHPt/m on elastase 1-promoted luciferase and Simian virus 40 T and t antigens (EL1-luc/TAg) transgenic mice, which spontaneously develop bioluminescent pancreatic adenocarcinoma due to two transgene constructs, simian virus 40 (SV40) T and firefly luciferase, regulated by the rat elastase 1 (EL1) promoter (30). The alterations of SV40 T on pathways of tumor suppression in p53 and retinoblastoma protein (31–33), which are relevant to human tumorigenesis, provide molecular, physiologic, and histologic aspects of tumorigenesis of acinar cell carcinoma (30). Moreover, by imaging the light emitted from the tumor cells, we can measure the tumor burden from otherwise indiscernible tissue locations and noninvasively quantify the antitumor activity of DACHPt/m from the same individual in real time. This also allowed us to avoid the variable onset of pancreatic tumor development, as previously reported for tumors mediated by expression SV40 T antigens (31–33). Our results showed that repeated systemic administration of DACHPt/m significantly inhibited the growth of pancreatic cancers and the incidence of metastasis in the EL1-luc/TAg transgenic mice by enhancing the accumulation of drugs in the tumors.

Results

In Vitro Cytotoxicity of DACHPt/m Against EL1-luc/TAg Cells. Oncogene expression leads to progressive growth of acinar cell carcinoma (30). Thus, after harvesting spontaneous tumor cells from 18-wk-old mice, we validated the in vitro cytotoxicity of DACHPt/m against these tumor cells and compared their activity against oxaliplatin, which is the only clinically approved carboxylato complex of DACHPt. In biological media, DACHPt/m and oxaliplatin produce similar reactive species, because the leaving group of DACHPt is displaced by H_2O and endogenous nucleophiles, such as Cl^- ions (34). Accordingly, the cytotoxic activity of DACHPt/m was as potent as the activity of oxaliplatin (Table 1), showing comparable IC_{50} values. In our previous study, such remarkably high cytotoxicity of DACHPt/m has been confirmed in several cell lines and demonstrated to be due to circumvention of drug inactivation by cytoplasmic detoxification proteins such as metallothionein and methionine synthase through the facilitated drug release from the micelles at the late endosome and lysosome (25).

Table 1. In vitro cytotoxicity of free oxaliplatin and DACHPt/m against EL1-luc/TAg tumor cells after a 48-h incubation

Drug	IC_{50}, μM
Oxaliplatin	39.2 ± 1.1
DACHPt/m	26.8 ± 1.7

IC_{50} values obtained from 3-(4,5-Dimethylthiazol-2-yl)-2,5-diphenyltetrazolium bromide (MTT) assay. Data are expressed as mean ± SEM (n = 4).

In Vivo Antitumor Activity of DACHPt/m Against Spontaneous Pancreatic Tumors. We tested the effect of DACHPt/m and oxaliplatin on spontaneous pancreatic tumors in EL1-luc/TAg mice. The treatment started when the mice were 13 wk old, and the intensity from the tumor had reached 1×10^6 photons per second. Mice were dosed with oxaliplatin at 2 and 4 mg/kg or DACHPt/m weekly at 2 mg/kg via i.v. injection for 8 wk. Imaging was done weekly. Quantification of the bioluminescence signal for each mouse is shown in Fig. 2*A*. The average bioluminescent signal in mice treated with DACHPt/m was 200-fold lower than that with saline after 8 wk, whereas the treatment with oxaliplatin at 2 mg/kg reduced the mean signal by only ~12-fold. Increasing the dose of oxaliplatin to 4 mg/kg resulted in several mice deaths, and the antitumor activity experiment was terminated at day 49, when only 30% of the mice were remaining. Representative bioluminescence images at weeks 0, 1, 3, 6, and 8 show much lower bioluminescence and restricted the dissemination in the peritoneal cavity for mice treated with DACHPt/m (Fig. 2*B*). The

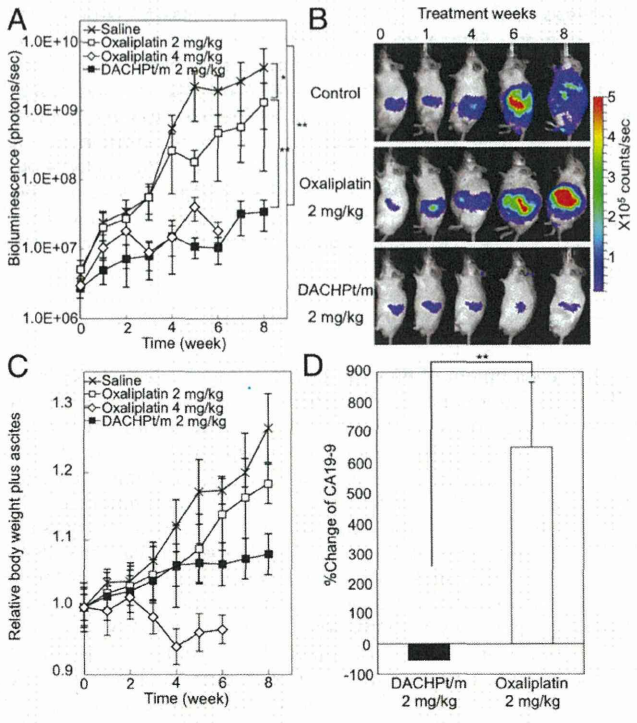

Fig. 2. Antitumor activity of DACHPt/m. (*A*) Male EL1-luc/TAg mice were imaged weekly from 13 to 21 wk of age. Longitudinal quantification analysis of bioluminescence signal of the EL1-luc/TAg mice treated with oxaliplatin or DACHPt/m. Crosses, saline; open squares, oxaliplatin at 2 mg/kg; open diamonds, oxaliplatin at 4 mg/kg; filled squares, DACHPt/m at 2 mg/kg). The units displayed on the *y* axis of this graph (measured flux) correspond to the sum of measured light from three positions (ventral and right and left flanks). Oxaliplatin at 4 mg/kg was followed until survival was 30% at day 49. (*B*) Bioluminescence of image of a representative mouse from saline-, oxaliplatin 2 mg/kg-, and DACHPt/m-treated groups. (*C*) Relative body weight including weight of ascites during the antitumor experiment. (*D*) Percent changes from baseline of serum CA19-9 after 28 d of treatment with oxaliplatin at 2 mg/kg and DACHPt/m at 2 mg/kg. Data are expressed as mean ± SEM (n = 10). *$P > 0.1$; **$P < 0.05$.

relative body weight of the mice including ascites showed a rapid increase for control and mice treated with oxaliplatin at 2 mg/kg, whereas it remained stable for DACHPt/m (Fig. 2*C*). Moreover, increasing the dose of oxaliplatin to 4 mg/kg resulted in ~10% of body weight loss (Fig. 2*C*), suggesting an aggravated toxicity at this dosage. It is reported that multiple administration of oxaliplatin at 4 mg/kg caused neuropathy, which is considered the dose-limiting side effect in the clinical situation (35), resulting in severe allodynia, 18% body weight loss, and high mortality (36).

The efficacy of DACHPt/m was also confirmed by measuring the levels of serum carbohydrate-associated antigen 19-9 (CA19-9) for evaluating the tumor burden, as it is a widely used tumor marker for diagnosis of pancreatic cancer as well as for measuring the effectiveness of cancer treatment by following the CA19-9 levels over time. CA19-9 is a monosialoganglioside (Sialyl Lewis^a) with high levels in various gastrointestinal malignancies, such as pancreatic, colorectal, gastric, and hepatic carcinomas (37). The presence of pancreatic adenocarcinomas in EL1-luc/TAg mice increased the CA19-9 levels, as observed in oxaliplatin-treated mice, whereas the reduction of CA19-9 levels for DACHPt/m corresponded to the improved prognosis. Accordingly, 28 d after starting the antitumor activity experiment, mice treated with oxaliplatin at 2 mg/kg augmented more than 600% of the mean level of CA19-9, whereas mice receiving DACHPt/m showed ~50% reduction of the average CA19-9, indicating a favorable prognosis in the mice treated with DACHPt/m ($P < 0.01$; Fig. 2*D*).

As the healthy pancreatic tissue of the EL1-luc/TAg transgenic mice also presents luciferase activity (30), we were not able to determine tumor regressions or study the disease-free survival. Therefore, we analyzed the increase of the luciferase expression by defining a significant threshold as the 10-fold increase of the bioluminescent signal at the beginning of the antitumor activity experiment, without spread of the bioluminescence to the body of the mice. Micelles maintained the bioluminescent signals from the pancreatic region, extending the 10-fold increase of bioluminescence ($P < 0.0001$; log-rank test), whereas the curve for the oxaliplatin group was comparable to that of nontreated mice (Fig. 3*A*). Remarkably, all mice in the DACHPt/m group were alive when the experiment was terminated at week 8, whereas only 50% of mice in the 2 mg/kg oxaliplatin group and 10% of mice in the 4 mg/kg oxaliplatin group remained at this time point (Fig. 3*B*). Moreover, ~80% of the mice treated with oxaliplatin showed liver and intestine metastasis and ascites during the study. However, only 2 of 10 mice treated with DACHPt/m presented small bioluminescent signal from metastasis in the liver, and no mice had metastasis in the intestine and ascites (Table 2). Thus, the overall survival, which was assessed until day 107 (62 d after the end of the treatment), was significantly improved by DACHPt/m (Fig. 3*B*; $P < 0.0001$, log-rank test).

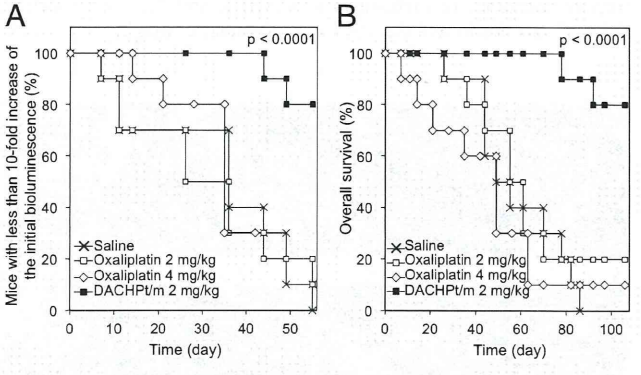

Fig. 3. Survival of EL1-luc/TAg mice. (*A*) Tenfold increase of bioluminescence, and (*B*) overall survival of mice without treatment, treated with oxaliplatin at 2 mg/kg and 4 mg/kg, and treated with DACHPt/m. Drugs were injected weekly. The 10-fold increase of the bioluminescence indicates the increase of the bioluminescent signal relative to the signal at the beginning of the antitumor activity experiment, without spread of the bioluminescence to the body of the mice. *P* value was calculated using the log-rank test.

Platinum Drug Accumulation in Spontaneous Pancreatic Tumors. The Pt accumulation in whole pancreas, that is, pancreas including tumor tissues, was studied 24 h after the injection of oxaliplatin or DACHPt/m. The accumulation levels of oxaliplatin in the pancreas having tumor tissues as well as in healthy pancreas were similar, showing ~2% of the injected dose per gram of tissue (Fig. 4), as oxaliplatin can penetrate and distribute in most tissues due to its small size (34, 38). In contrast, DACHPt/m exhibited increased accumulation in the pancreas having tumor tissues due to the EPR effect, whereas showing lower accumulation in the pancreas of wild-type mice even compared with free oxaliplatin, due to the restricted penetration in healthy tissues with continuous vascular endothelium because of their size and stability in the bloodstream (Fig. 4). The targeting efficiency of the micelles to the tumor was estimated by taking the ratio of the accumulated dose in the pancreas in transgenic mice versus the accumulated dose in the pancreas of wild-type mice. Accordingly, DACHPt/m achieved a threefold higher accumulation ratio, suggesting that the micelles can increase the accumulation of the drug at the tumor site.

Intratumoral Microdistribution of DACHPt/m. By H&E staining of the tumor tissue, we observed cells with moderate pleomorphism, round nuclei, and abundant eosinophilic cytoplasm and apparent mitotic activity (Fig. 5*A*). The cells form acinar and trabecular structures, adopting a solid growth pattern in certain areas. Moreover, numerous vessels with prominent endothelium are observed. Staining vascular endothelial cells with anti-platelet endothelial cell adhesion molecule (PECAM1) antibody suggests a high vascular density (Fig. 5*B*, green). Moreover, the tumor sections may present occasional pericytes, marked with anti-PDGF receptor β antibodies (Fig. 5*B*, blue) and antismooth muscle actin (SMA) antibodies (Fig. 5*B*, red), surrounding the perivascular regions.

Fluorescent-labeled DACHPt/m were injected into EL1-luc/TAg transgenic mice to study the microdistribution of the micelles in the tumors. Accordingly, 24 h after the injection, tumor tissues were excised and studied by immunofluorescence. The fluorescence of the micelles was broadly distributed in the tissue sections (Fig. 6, magenta), and far from the blood vessels (Fig. 6, green), indicating that the micelles successfully penetrated within the whole tumor.

The microdistribution of DACHPt delivered by the micelles in healthy pancreas and tumor tissues was determined by using μ-synchroton radiation–X-ray fluorescence (μ-SR-XRF). μ-SR-XRF allows studying histological characteristics by tracing the elements originally present in animal tissues, while evaluating the microdistribution of the drugs by mapping the exogenous Pt atoms. Thus, the distribution of Fe atoms, which are present in hemoproteins, matched the distribution of blood vessels in tumor tissues and healthy pancreas (Fig. 6). The Pt mapping of

Table 2. Presence of metastases and ascites of mice ($n = 10$) after 8 wk of treatment with weekly i.v. injections of free oxaliplatin at 2 mg/kg and DACHPt/m at 2 mg/kg

	Metastasis		
Group	Liver	Intestine	Ascites
No treatment	8/10	7/10	8/10
Oxaliplatin	8/10	7/10	9/10
DACHPt/m	2/10	0/10	0/10

Metastasis from bioluminescent imaging.

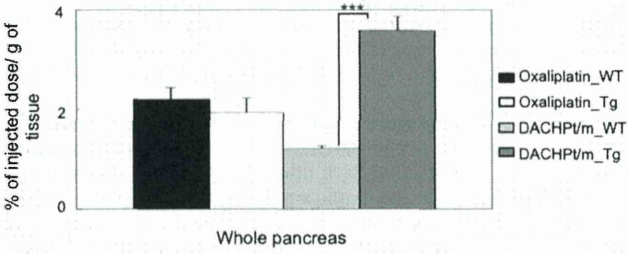

Fig. 4. Accumulation of oxaliplatin and DACHPt/m in whole pancreas including pancreatic tumors of EL1-luc/TAg mice 24 h after injection. Accumulation of drugs in pancreas of wild-type mice was taken as reference. Data are expressed as mean ± SEM ($n = 5$). ***$P < 0.01$.

the tissues showed that DACHPt/m deeply penetrated and delivered the drug in the pancreatic tumors, whereas, in healthy pancreas, the micelles were confined to the blood vessels, as indicated by the high colocalization of Pt and Fe, because of their continuous vascular endothelium.

Discussion

Our results confirmed the efficacy of DACHPt/m against a transgenic pancreatic tumor model as they limited the growth of primary tumors and reduced the development of metastases and ascites, greatly extending the survival of mice. This survival was prolonged well beyond the treatment period, despite the fact that SV40 T oncogene is continuously expressed in EL1-luc/TAg transgenic mice (30), which allows tumors to regrow after termination of therapy, limiting the long-term survival. This control of the disease did not come at the expense of side effects, and the repeated administration of DACHPt/m, i.e., once a week for 8 wk, suggests that micelles can be used for prolonged chemotherapy cycles.

We have previously reported the efficacy of DACHPt/m against various xenografted tumor models (24–27). These studies demonstrated that the enhanced accumulation of DACHPt/m in the malignancies, through the EPR effect, leads to the suppression of the growth rate of the tumors. However, these models did not allow us to follow the antitumor effects for prolonged periods and assess clinically meaningful survival rates and dose schedules. Moreover, the immune responses, tumor microenvironments, cellular subpopulations, and metastatic cascades, which are severely altered in xenograft models, may affect the efficiency of the drugs. Conversely, EL1-luc/TAg transgenic mice used in this study present gradual cancer development and metastasis, following physiological events of neoplastic progression and tumorigenesis under a viable immune system, consistent with the evolution of human pancreatic cancers. Thus, the transgenic tumor model facilitated testing clinically significant dosages, in conditions close to the real setting of the disease.

This model has been previously used for the evaluation of rapamycin (30), a mammalian target of rapamycin inhibitor that regulates cell growth, progression of cell cycle, and tumorigenesis (39), showing suppression of the carcinoma development. However, the inhibitory effect of rapamycin was inconstant, and some EL1-luc/TAg transgenic mice circumvented its therapeutic action (30). Conversely, DACHPt/m presented a strong antitumor effect, which was reproducible among all mice, showing reduced individual variability. As both DACHPt and oxaliplatin form platinum–DNA adducts, which activate several cellular processes that mediate their cytotoxicity, and their in vitro cytotoxicity against the cancer cells harvested from the spontaneous tumors was comparable, the higher efficacy of DACHPt/m may be associated with their enhanced accumulation in the pancreatic tumors.

The penetration and retention of systemically injected DACHPt/m within the transgenic pancreatic tumors resulted in their increased tumor accumulation. Of note, EL1-luc/TAg transgenic mice may develop tumors with pericyte-covered vasculature, which has been strongly associated with reduced penetration of macromolecules and nanocarriers in solid tumors (40, 41). Twenty-four hours after injection, DACHPt/m were found broadly distributed within the tumors, which can be associated with the prolonged blood circulation and high stability in the bloodstream of the micelles (24–26), as well as their densely PEGylated shielding and their relatively small diameter (30 nm) (25, 26). By using intravital microscopy, we have recently found that DACHPt/m maintained their micelle form during their circulation in the bloodstream and penetration into solid tumors (25), whereas the size of the micelles was critical for achieving deep penetration, particularly in poorly permeable malignancies, such as pancreatic tumors, with 30-nm diameter DACHPt/m being capable of passing through the vasculature and interstitium and deeply penetrating inside the tumors (26). Hence, in conventional chemotherapy using oxaliplatin, the gradients of drug concentration in the tumor may cause the cells far from the vasculature to receive sublethal doses, leading to the development of drug resistance (42, 43). In contrast, we hypothesized that, by using DACHPt/m, most tumor cells may be exposed to therapeutic concentrations of the drug, improving the scenario of tumor recurrence and resistance to the therapy.

Spontaneous tumors are a powerful tool for design validation, determination of mechanisms of action, and preclinical assessment of nanotechnology-driven approaches for their translation into efficient therapies for cancer patients. Such models can be induced environmentally by causing genetic and epigenetic alterations in cells, which become genomically unstable and transformed into neoplastic cells, or by genetically engineering the host to produce tissue-specific tumors (6, 7). Although several nanocarriers have been evaluated on environmentally induced models (44–46), these models are usually limited to tissues with large surface exposure to the agents, and they embody subgroups of tumor types and grades, which may not represent actual tumors (6, 7). Conversely, genetically engineered models are particularly suited for testing nanocarriers as they promote stepwise molecular and cellular events resulting in malignancies with close interactions with immune cells, vascular and lymphatic networks, and the extracellular matrix (6, 7). Moreover, whereas the therapeutic effect of nanocarriers on transgenic tumor models has been assessed by endpoint analysis (13) or indirectly measuring the tumor burden by computed tomography (14), in this study, we were able to match initial tumor burden between groups, monitor the progression of tumors, incidence of metastases and ascites, and the antitumor activity of micelles in real time by bioluminescence imaging due to the

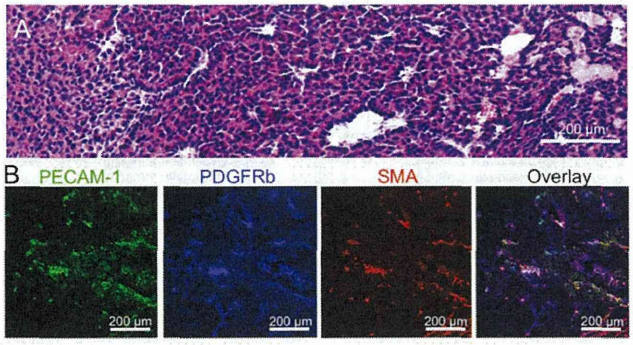

Fig. 5. Histology of EL1-luc/TAg transgenic mouse. (*A*) H&E staining and (*B*) immunohistochemistry of pancreatic tumor from EL1-luc/TAg. Examination revealed areas rich in blood vessels (PECAM1, green) slightly surrounded by pericytes (PDGFRb, blue and SMA, red).